Sedimentary and mineral dust sources of dissolved iron to the World Ocean

J. K. Moore, O. Braucher

Biogeosciences Discuss., 4, 1279–1327, 2007
www.biogeosciences-discuss.net/4/1279/2007/

Biogeosciences Discussions is the access reviewed discussion forum of *Biogeosciences*

Sedimentary and mineral dust sources of dissolved iron to the World Ocean

J. K. Moore[1] **and O. Braucher**[1,*]

[1]University of California, Irvine, Department of Earth System Science, Irvine, CA 92697-3100, USA
[*]now at: Humboldt State University, Arcata, CA, 95521, USA

Received: 22 March 2007 – Accepted: 6 April 2007 – Published: 25 April 2007

Correspondence to: J. K. Moore (jkmoore@uci.edu)

Abstract

A worldwide database of dissolved iron observations is used to improve simulations of the marine iron cycle within a global-scale, Biogeochemical Elemental Cycling (BEC) ocean model. Modifications to the model include: 1) an improved particle scavenging parameterization based on the sinking mass flux of particulate organic material, biogenic silica, calcium carbonate, and mineral dust particles; 2) desorption of dissolved iron from sinking particles; and 3) an improved sedimentary source for dissolved iron. Most scavenged iron (90%) is put on sinking particles to remineralize deeper in the water column. The model-observation mismatches are greatly reduced both in surface waters and in the deeper ocean. Inclusion of desorption has little effect on surface water iron concentrations where adsorption/scavenging is strongly dominant, but significantly increases simulated iron concentrations in the deep ocean. Our results suggest that there must be substantial removal of dissolved iron from subsurface waters (where iron concentrations are <0.6 nM in most regions) to match observed distributions. Aggregation and removal on sinking particles of Fe bound to organic colloids is a likely mechanism.

The improved BEC model is used to address the relative contributions of mineral dust and marine sediments in driving ocean productivity and observed dissolved iron distributions. The sedimentary iron source from the continental margins has a strong impact on open ocean iron concentrations, particularly in the North Pacific. Plumes of elevated dissolved iron concentrations develop at depth in the Southern Ocean, extending from source regions in the SW Atlantic and around New Zealand. The lower particle flux and weaker scavenging in this region allows the continental iron source to be advected far from source areas. Both the margin sediment and mineral dust Fe sources significantly impact global scale primary production, export production, and nitrogen fixation, with inputs from dust deposition having a modestly stronger impact. Ocean biogeochemical models need to include the sedimentary source for dissolved iron, or they will overestimate the impact of dust deposition variations on the marine

BGD

4, 1279–1327, 2007

carbon cycle.

1 Introduction

Iron has been recognized as a key micronutrient, limiting phytoplankton growth in the oceans, beginning with field measurements and bottle incubation experiments (i.e., Martin et al., 1991) and later through in situ iron fertilization experiments (Coale et al., 1996; 2004; Boyd et al., 2000; Tsuda et al., 2003; see review by de Baar et al., 2005). Limitation of phytoplankton community growth rates are seen in three High Nitrate, Low Chlorophyll (HNLC) regions in the Southern Ocean, and the subarctic and equatorial Pacific, with strong iron-limitation of the larger diatoms, and weaker iron-limitation and strong grazing pressure on the smaller phytoplankton (Price et al., 1994; de Baar et al., 2005, and references therein). In addition, the nitrogen fixing phytoplankton may often be iron-limited in subtropical and tropical waters where most of the phytoplankton community is limited by available nitrogen (Falkowski, 1997; Michaels et al., 2001; Berman-Frank et al., 2001; Moore et al., 2004, 2006). Thus, rates of iron input to the oceans may ultimately control global marine productivity, modifying production directly in the HNLC regions and indirectly in the subtropical gyres and other low latitude areas by modifying rates of nitrogen fixation (Falkowski 1997; Michaels et al., 2001; Gruber, 2004; Moore et al., 2006; Moore and Doney, 2007).

Iron has been incorporated as a limiting nutrient for phytoplankton growth in a number of global-scale ocean biogeochemical models (Archer and Johnson, 1999; Moore et al., 2002, 2004; Aumont et al., 2003; Gregg et al., 2004; Parekh et al., 2004; 2005; Doney et al., 2006). These efforts were made possible by growing understanding of iron cycling in the oceans, the result of numerous field campaigns, including those associated with the international Joint Global Ocean Flux Study and the iron fertilization experiments (see Doney and Ducklow, 2006; and de Baar et al., 2005; and references therein). The treatment of iron in these models is still rudimentary, with a single dissolved pool and typically no explicit iron-ligand interactions (some ligand dynamics in

BGD
4, 1279–1327, 2007

EGU

Parekh et al., 2004, 2005; and Doney et al., 2006), due to the remaining large uncertainties associated with the sources and sinks of iron-binding ligands, the relative bioavailability of ligand bound iron, and the interaction of ligands with particle scavenging removal of dissolved iron. Parekh et al. (2004) examined three different models of iron cycling in the context of an ocean box model that included: 1) a net scavenging onto particles; 2) a scavenging and desorption model; and 3) an explicit ligand complexation model (with globally uniform ligand concentration at 1 nM) that applied scavenging only to the free Fe ion.

It has been recognized that the flux of iron from the sediments, including in sediment re-suspension events, leads to high iron concentrations in coastal waters (Luther and Wu, 1997; Johnson et al., 1999, Chase et al., 2005). However, it has generally been assumed that dissolution from mineral dust was the main source of dissolved iron to the open ocean (i.e., Jickells et al., 2005), particularly in the development of ocean biogeochemical models, most of which include only a dust source for dissolved iron (Archer and Johnson, 1999; Aumont et al., 2003; Gregg et al., 2004; Parekh et al., 2004, 2005). Moore et al. (2004) included a constant sedimentary iron source of 2 μmol Fe/m^2/day in areas where depth was less than 1100 m. However, due to the coarse grid resolution and the necessary strong smoothing of ocean bathymetry, this iron source was often too deep to influence surface ocean biogeochemistry, even in grid locations directly adjacent to the continents (Moore et al., 2004). Thus, the biogeochemical impact of this iron source was greatly underestimated.

Several papers have suggested that the iron source from the continental margin sediments may significantly impact global iron distributions, including production and export in waters far offshore. In the Southern Ocean, rapid advection of iron from sedimentary sources in the SW Atlantic within the Antarctic Polar Front was suggested to account for high iron concentrations measured along 6° W (de Baar et al., 1995; Löscher et al., 1997). Johnson et al. (2003) noted the influence of the continental iron source extending well into the North Pacific subtropical gyre. Elrod et al. (2004) estimated a very large input of dissolved iron from continental shelf sediments of 8.9×10^{10} mol

BGD
4, 1279–1327, 2007

Fe/yr based on benthic chamber flux data (Berelson et al., 1996, 2003). They suggested the sedimentary source is at least as large as the inputs of soluble iron from mineral dust, and noted the apparent continental shelf influence extended hundreds of km offshore. They also found a strong relationship between iron release and organic carbon oxidation in the sediments, indicating sediments beneath productive regions should have significantly higher release of dissolved iron (Elrod et al., 2004). Johnson et al. (2005) found strong offshore transport of dissolved iron by eddies into the gulf of Alaska. Lam et al. (2006) found evidence for offshore advection of particulate and dissolved iron from the margin over 900 km to Station P in the gulf of Alaska. In their review of iron distributions in the oceans, de Baar and de Jong (2001) noted the high concentrations of iron often observed close to the continental margins, with the impact of this source often extending far offshore.

In a companion paper, we present a new database of dissolved iron distributions throughout the world ocean, noting a strong apparent influence of the continental iron source with high values near the continental margins and steadily decreasing offshore (Moore and Braucher, this issue, hereafter referred to as MBa). In this paper we attempt to improve several key aspects of iron cycling in the Biogeochemical Elemental Cycling (BEC) model, including an improved sedimentary source for dissolved iron. The BEC model includes several key phytoplankton functional groups (diatoms, coccolithophores, diazotrophs, and picoplankton) and the biogeochemical cycles of key elements (C, N, P, Fe, Si, and O). The observational database is used to evaluate and constrain the model. We then use the improved model to examine the relative roles of the sedimentary and mineral dust sources for dissolved iron in driving oceanic dissolved iron distributions and the marine biogeochemical cycles of carbon and nitrogen.

2 Methods

The biogeochemical elemental cycling (BEC) model used here includes an ecosystem component with four phytoplankton functional groups (diatoms, diazotrophs, picophy-

toplankton and coccolithophores), multiple potentially growth limiting nutrients (nitrate ammonium, phosphate, dissolved iron, and silicate), and one zooplankton group. The coccolithophores are simulated as a dynamically varying fraction of the small phytoplankton group. The model also tracks the distributions of dissolved organic matter, dissolved inorganic carbon, dissolved oxygen, and alkalinity. Sinking particles of particulate organic matter (POM), particulate iron (pFe), biogenic silica (bSi), calcium carbonate ($CaCO_3$), and mineral dust are treated implicitly, assumed to sink and remineralize at the same location where they are formed (Moore et al., 2004), where the remineralization profiles are determined from the mineral ballast model of Armstrong et al. (2002). The BEC model runs within the ocean circulation component of the Community Climate System Model (CCSM, Collins et al., 2006; Yeager et al., 2006). The BEC model has been described in detail elsewhere (Moore et al., 2002, 2004; Moore and Doney, 2007). Here we focus on key aspects of iron cycling in the model relevant to the present study (see also MBa, this issue).

The phytoplankton groups have a variable Fe/C ratio that changes dynamically as a function of ambient dissolved iron concentrations, allowing a decrease in the ratio under low iron concentrations. The optimum Fe/C ratio is set at 6 μmol/mol for all groups except the diazotrophs, which have a higher ratio of 40 μmol/mol. These ratios can decline to values of 3 μmol/mol and 15 μmol/mol under strongly iron-limiting conditions (see Moore et al., 2004 for details). In the companion paper we showed that the model tends to overestimate surface iron concentrations in the standard configuration. In this work, we lower the half-saturation constants for iron uptake in part to address this deficiency, to values of 0.04 nM for the small phytoplankton, 0.06 nM for the diazotrophs, and 0.09 nM for the diatoms. These values are within the range reported in the literature. A half-saturation constant of 0.035 nM was estimated for community uptake in the tropical Pacific (Price et al., 1994). The rates for large diatoms are often significantly higher than our value (>0.2 nM, Timmermans et al., 2004; de Baar et al., 2005) but lower rates have been observed for smaller diatoms from HNLC regions (0.12 nM for the Iron Ex II diatom dominated bloom, Fitzwater et al., 1996; diatom values of 0.05–

0.13 nM for the Ross Sea, Coale et al., 2003). Kudo et al. (2006) estimated values of 0.10 nM and 0.08 nM for the micro and nano-sized phytoplankton fractions in the SERIES experiment in the NW subarctic Pacific.

2.1 Improving the BEC iron scavenging parameterizations

We began by modifying some of the basic assumptions of the iron scavenging parameterizations of Moore et al. (2004). Typically ocean biogeochemical models assume that 100% of the dissolved iron scavenged onto particles is lost to the sediments (Moore et al., 2002; Christian et al., 2002; Aumont et al., 2003; Parekh et al., 2005). This is unrealistic as most of the particles scavenging iron in the upper water column will not even reach the ocean floor but remineralize in the upper ocean releasing the iron. Moore et al. (2004) put 10% of the scavenged iron into sinking particulates and allowed it to remineralize within the water column. Here we increase this fraction to 90%. The remaining 10% is assumed lost to the sediments and provides the ocean sink necessary to balance inputs from the atmosphere and the sediments (the model does not include a sedimentary diagenesis component). This more realistic treatment of scavenged iron allows the dust deposition (and sedimentary iron) signal to penetrate deeper into the ocean as iron is scavenged, released, then scavenged again down the water column.

We also increased the fraction of sinking dust particles that reach the ocean floor from ~85% to ~92% over a 4000 m water column. The remineralization length scale for the "hard" dust fraction (97% of the dust that enters the ocean as sinking particulates) is increased from 40 000 m to 120 000 m. Thus, only about ~3% would dissolve over a 4000 m water column (see Armstrong et al., 2002 and Moore et al., 2004 for details of the particle remineralization scheme). The remaining 3% that enters the ocean as sinking particulates is remineralized in the upper water column with a length scale of 600 m. Two percent of the dust flux is assumed to dissolve instantaneously upon deposition to the oceans. Biogeochemical models typically include only this surface dissolved iron input flux. However, it seems likely that some slow additional dissolution of iron occurs as dust particles sink through the water column, particularly within

BGD
4, 1279–1327, 2007

low pH microenvironments in aggregates or zooplankton guts, and through biological "stripping" of iron from particles as suggested by the recent FeCYCLE field experiment results (Frew et al., 2006). The three percent that dissolves in the upper water column reflects the fact that these biological processes are weighted towards the surface ocean following the general distributions of organic material and zooplankton biomass. Dust deposition is from the climatology of Luo et al. (2003).

Moore et al. (2004) scaled iron scavenging by the sinking particle flux of particulate organic carbon (POC) plus mineral dust. Here we use a modified definition of sinking particle mass flux in conjunction with a first order scavenging coefficient (Febase = 3.84e-3 day^{-1}), where the sinking mass = POC * 6 + biogenic silica (bSi) + $CaCO_3$ + mineral dust (all in units of ng/cm^2). Unlike in Moore et al. (2004), no maximum scavenging rate is imposed. Sinking mass flux in the deep ocean is dominated by the mineral ballast components (bSi, CaCO3, and lithogenic, Armstrong et al., 2002; Klaas and Archer, 2002). Thus their inclusion allows the model to more accurately capture the sinking flux available to scavenge iron in the deep ocean. Sinking flux in the upper ocean is strongly dominated by the particulate organic matter (POM), which decreases more rapidly with depth due to a shorter remineralization length scale. The POC flux is multiplied by a factor of 6 to reflect the non-carbon portions of organic matter, and to reflect an increased scavenging efficiency in the upper ocean due to higher particle concentrations, "stickier" freshly produced organic material, and more colloidal organic material (COM) thought to be important in trace metal scavenging, all of which likely scale to first order with POC flux and biological activity. Recent studies point to a strong influence of COM on the scavenging and removal of ^{234}Th from upper ocean waters, and perhaps throughout the water column as organic coatings on the mineral substances sinking through the water column (Guo et al., 2002; Passow et al., 2006; see review by Santschi et al., 2006). Similar processes likely influence the scavenging and removal of iron. We note that in reality the specific organic coatings and particle size distributions will strongly influence trace metal scavenging (i.e. Burd et al., 2000; Savoye et al., 2006). These factors are not simulated in the model and

BGD
4, 1279–1327, 2007

here we propose a bulk formula that attempts to parameterize these effects as a net scavenging onto the sinking particles. Thus, our approach is similar to the simplest models of thorium scavenging (see review by Savoye et al., 2006) except that we do include an explicit desorption of iron from the sinking particles (see below).

We also increase scavenging rate rapidly as dissolved iron concentrations exceed 0.6 nM, implicitly including the ligand effect as in Moore et al. (2004). Thus, we assume that almost all of the iron at concentrations less than 0.6 nM will be bound to organic ligands and have reduced scavenging loss rates. Unlike in previous work, however, scavenging rates are not progressively reduced as ambient iron falls to lower concentrations. In the companion paper we suggested that this led the BEC model to overestimate iron concentrations at lower ambient levels (<~0.3 nM, MBa, this issue). Here we demonstrate that a much better match to observations is obtained if scavenging where iron is less than 0.6 nM is simply a first order rate function of the sinking particle mass. Also, new in this work is a desorption release of dissolved iron from sinking particles, based on a first order rate constant as suggested for Th (Bacon and Anderson, 1982) and applied to iron by Parekh et al. (2004). As sinking particles are implicit in the model and assumed to instantly sink and remineralize through the water column at the same location where formed (Moore et al., 2004), this rate is not expressed in units of time, but rather length (6.0e-6 cm^{-1}). This can be converted to the more familiar time units if we assume some mean sinking speed (at 100m/day the desorption rate would be 0.06 day^{-1}). Parekh et al. (2004) examined desorption rates between 0.055–0.27 day^{-1}). Desorption is only applied to the particulate Fe sinking pool coming from particle scavenging and biological uptake and export, not to the inert Fe in the non-dissolving portion of the mineral dust particles. We conduct two sensitivity simulations to examine the impact of this desorption on iron distributions (see below).

We also modify the sedimentary source for iron in the model. Moore et al. (2004) included a simple sedimentary source of 2 μmol/Fe/m^2/day everywhere that ocean depth on the coarse-resolution model grid was less than 1100 m. This improved the model

BGD
4, 1279–1327, 2007

results in some areas (like the Ross Sea for example), allowing the model to capture observed phytoplankton blooms in otherwise HNLC areas. However, as noted by Moore et al. (2004) the sedimentary source was only weakly captured due to the coarse resolution of the grid and the necessary smoothing of bottom topography. Thus, in some areas where shelf sediments are known to be important sources of iron, like the U.S. west coast (Johnson et al., 1999), the bottom level of the ocean model was often much deeper than 500 m, even in grid cells directly adjacent to the continent. Thus, very little of the iron released in the bottom grid cell reached surface waters to influence biological production. To correct for this problem, here we use a sedimentary source that is weighted by the actual ocean bathymetry from the ETOPO2 version 2.0 2-min global gridded database (U.S. Dept. of Commerce, 2006). Thus, for each cell in the model, we calculate what fraction of the cell area that would consist of sediments based on the high resolution ETOPO2V2 database (what portion of the ocean floor in ETOPO2V2 had depths that lie within that grid box). This effectively decouples the sediment source from the physical ocean grid, and provides for a much more realistic distribution of the sedimentary iron source. Figure 1 shows the percentage area with sedimentary flux integrated through the upper 281 m from the old scheme (100%, only in bottom ocean grid cell) compared with the new sedimentary source based on the ETOP2V2 dataset. It can be seen that the influence of the continental shelves are much better accounted for in many areas where they previously had no influence on sedimentary iron flux in the upper ocean. In addition, important iron sources surrounding islands in the open ocean are represented, such as the shallow waters associated with the Kerguelen Plateau and Kerguelen Islands (70° E, 50° S, see Moore and Abbott, 2000; Blain et al., 2001).

We also employ a more sophisticated estimate of the Fe flux from sediments than the constant value used previously. Elrod et al. (2004) found a strong correlation between iron release from sediments and organic carbon oxidation in the sediments (0.68 μmol Fe/mmol C_{ox}/m^2/day) using benthic flux chamber data off the N. American west coast from Berelson et al. (1996, 2003). We simplify this relation using 0.68 μmol Fe/m2/day

BGD
4, 1279–1327, 2007

release for each mmol of C m^2/day sinking into the ocean grid cell where sedimentary flux is being calculated. This iron flux is then weighted by the % sedimentary area computed from the ETPO2V2 data. Initially, the sedimentary iron flux was determined by the sinking C fluxes from year 3000 of the Old BEC simulation (see below). As this iron input can modify the organic carbon export, an initial simulation with the iron cycle modifications was run for 20 years, and then the sedimentary flux was re-computed based on the sinking organic C flux from year 20 and used in all subsequent simulations. Ideally the iron flux could be dynamically, linked with the sinking POM flux in the context of a sedimentary diagenesis model. There is no explicit depth dependence on the sedimentary iron source, it is a function of only the sinking POC fluxes (thus there are much higher iron fluxes beneath productive continental margins, and even in the deep ocean there is a small source). Elrod et al. (2004) noted a delay between organic matter flux and iron release from the sediments of several months. We make the simplifying assumption of a constant flux based on the annual sinking POC flux. In several regions the resulting Fe sediment flux grid was modified to correct mismatches between the ETOPO2V2 and CCSM3 grids and to better match local bathymetry maps and dissolved iron measurements (Mackey et al., 2002; Reddy and Arrigo, 2006; Bruland et al., 2005).

Given the assumptions and modifications to the model outlined above, we optimize the other parameters in the BEC iron cycle to best match the dissolved iron concentrations from our observational database (MBa, this issue) by minimizing the root mean square difference of the log-transformed model output and observational values. The first order scavenging rate (Febase = 0.00384 day^{-1}) was optimized by comparisons with both euphotic zone (0–103 m) and subsurface observations of dissolved iron (103–502 m, there are few observations below 502 m depth). Arguably, the subsurface observations are preferable for this parameter tuning as they are less affected by the uncertainties associated with surface inputs and biological uptake of dissolved iron. However, there are far more observations in surface waters than subsurface (MBa, this issue). Somewhat reassuringly, the optimal value for Febase was similar for euphotic

zone and subsurface waters (~6% higher for subsurface waters), implying a similar dependency on sinking particle flux. This was not the case for the coefficient (Chigh) used in the equation increasing particle scavenging at high iron concentrations (see MBa, this issue). The optimal value for surface waters was a factor of 3–4 higher than in subsurface waters. For our new optimized parameter set we use an intermediate value (Chigh=3300) that gave similar rms model-data differences in surface and subsurface waters for high-end iron concentrations (where both model and observation exceeded 0.6 nM). We will show that this leads to a positive model bias in surface waters and a negative bias in subsurface waters where iron concentrations are on the high-end (>0.6 nM). The new iron scavenging parameterization is summarized in Eqs. (1)–(3) below, where the scavenging rate is given by Febase * the sinking mass flux, and is increased under high iron conditions (above HighFe = 0.6 nM). The scavenged iron is removed from the dissolved pool and 90% is put into sinking particulate iron (10% is presumed lost to the sediments).

$$\text{ScavRate}=\text{Febase} * (\text{POCx6} + \text{Dust} + \text{bSi} + \text{CaCO3}) \quad (1)$$

$$\text{If dFe} > \text{HighFe then ScavRate}=\text{ScavRate} + (\text{dFe}-\text{HighFe}) * \text{Chigh} \quad (2)$$

$$\text{ScavengedIron}=\text{dFe} * \text{ScavRate} \quad (3)$$

We compare BEC model results with the modifications outlined above optimized with the observational dataset (New BEC), with the last year from an earlier 3000 year equilibrium simulation (the "Control" simulation described by Moore and Doney, 2007, and compared with observations by MBa (this issue) here referred to as the "Old" BEC). The New BEC simulation was 201 years, long enough for the iron cycle to spin up with a reasonably small drift (0.025% per decade drift in global mean iron concentration over the last 20 years, a drift of 0.0024% per decade in the upper 502 m). We focus on model output from year 201. To gauge the sensitivity to iron sources we compare with two additional 201 year simulations; one with only dust inputs of dissolved iron (DustOnly) and one with only sedimentary inputs of dissolved iron (SedOnly). We conduct

several other sensitivity simulations: 1) NoDesorp – does not include Fe desorption from sinking particles; 2) LowFe – a low-end estimate of iron inputs, with a 1% surface dissolution of the iron in mineral dust as the only source; 3) HighDesorp – desorption rate is increased by 33% to 8.0e-6 cm^{-1}, and the base scavenging rate is increased to 0.00395 day^{-1}. In the LowFe simulation particle scavenging of iron occurs only where iron concentration exceeds 0.6 nM. Except for these noted differences, all the sensitivity simulations are identical to the New BEC simulation. Atmospheric forcings for all simulations are from a from a late 20th century NCAR-NCEP climatology (Large and Yeager, 2004).

To evaluate the simulations against the observational database and tune model parameters we log transform the observations and model output and then compute the correlation coefficient (r) and the root mean square (rms) difference. Log transformation provides for a more equal weighting of model-data differences across the relatively wide range of iron concentrations (rather than weigh high-end values much more strongly than low iron values without log transformation).

3 Results

The total dissolved iron inputs to the oceans from our improved sedimentary source (2.0e10 molFe/yr) is of similar magnitude as the total inputs from mineral dust (2.4e10 molFe/yr, Fig. 2). The sedimentary source is mainly coming from the continental margins at relatively shallow depths (81%<502 m, compare Figs. 2b and d). More of the total release from mineral dust is in the deep ocean (42%>502 m). After 201 years, the combined dust and sediment sources are balanced by the 10% of scavenged iron that is lost to the sediments (Fig. 2c). Comparing the spatial patterns seen in Fig. 2, it is apparent that much of the iron input in the high dust deposition regions in the North Atlantic and North Indian oceans, and along the continental margins is lost to scavenging locally before the circulation can advect it very far. Our estimate for sedimentary dissolved iron input is somewhat lower that the value of 8.9e10 molFe/yr

BGD
4, 1279–1327, 2007

of Elrod et al. (2004). This difference is likely due to our use of model simulated organic carbon export (typically lower than observations on the continental shelves) to estimate the iron flux. Previous estimates for dissolved iron inputs from dust, typically only including a surface dissolution include 9.6e8–9.6e9 molFe/yr (Fung et al., 2000) 2.4e9 molFe/yr (Aumont et al., 2003), 3.75e10 molFe/yr (Moore et al., 2004), and 2.6e9 molFe/yr (Parekh et al., 2005). Recently estimates based on higher surface solubilities for the iron in mineral dust have led to estimates of 2.0e10–8.9e10 molFe/yr (Luo et al., 2005) and 1.3e11 molFe/yr (Fan et al., 2006).

We next compare the simulated iron concentrations and distributions from the Old BEC simulation with those from the New BEC simulation in the context of the observational database. The observations from surface waters (0–103 m) and from subsurface waters (103–502 m) are compared with the simulated values in Fig. 3, where the model output has been sub-sampled from the same month, location, and depth as the observations. In the companion paper, we noted a strong tendency for the Old BEC to overestimate iron concentrations at lower iron values in the open ocean subset (<~0.3 nM, MBa, this issue). The same pattern is apparent here in the full observational dataset (Figs. 3a and c). This tendency is greatly reduced in the New BEC simulation, which did not include the progressive decrease in scavenging rates at low iron concentrations used in the Old BEC model (Figs. 3b and d). Thus, a first order dependence on sinking particle concentration (where iron <0.6 nM) provides a much better fit to the observations. In general, the New BEC simulation is greatly improved relative to the observations with the log-transformed, r-correlation value increasing from 0.40 to 0.62 (+57%) in surface waters (Figs. 3a and b), and from 0.49 to 0.63 (+29%) in subsurface waters (Figs. 3c and d). Similarly, the root mean square difference (after log-transformation) between simulated and observed iron values is reduced in the New BEC simulation by 17% in surface waters and by 10% in subsurface waters (Fig. 3). The basin scale patterns seen in Fig. 3 with high values in the North Indian and North Atlantic oceans and lower values in the Southern Ocean, are discussed in detail in the companion paper (MBa, this issue).

BGD
4, 1279–1327, 2007

The largest data-model mismatch in the Old BEC simulation comes from data collected along the west coast of South America by Bruland et al. (2005) that strongly reflects iron input from sedimentary sources on the continental margin (the black diamonds in the lower right corner of Fig. 3a). This mismatch is much reduced in the New BEC simulation (Fig. 3b). Many of these data points fall in a straight line (constant iron concentration) in the BEC model output. This is the result of high resolution onshore-offshore transects, where multiple measurements were made that fall within a single grid box of the BEC model. This highlights one difficulty of comparing field observations with the model output. Somewhat apparent in Figs. 3b and d is the tendency for the model to overestimate in surface waters and underestimate in subsurface waters the high-end iron concentrations (>0.6 nM).

Comparing Figs. 3b and d, it can be seen that there is considerably greater scatter around the one-to-one line (and higher rms difference) in surface waters than in subsurface waters. This largely reflects the uncertainties associated with the biological uptake and removal from the euphotic zone. This removal is impacted by numerous parameters in the model including the half-saturation values for iron uptake by the different phytoplankton groups. Other factors such as mixed layer depths and upwelling rates, the concentrations of the other nutrients also impact this biological removal in surface waters. Thus, the subsurface iron concentrations may be a better indicator of how well the scavenging parameterizations for iron are working in the model. In this respect, the relatively narrow spread around the one-to-one line, low rms difference, and good correlation with observations seen in Figure 3D are encouraging.

Basin mean iron concentrations from the observations are compared with the New and Old BEC values (where again model output has been sub-sampled at the same month, location, and depth of each observation) in Table 1. Deep ocean values (>502 m) in the North Atlantic and North Pacific in the New BEC simulations are closer to the observed values than in the Old BEC simulation, but still too low. The New BEC simulation is much closer to observed values in the open ocean, surface waters of the Southern Ocean, equatorial, South, and North Pacific (Table 1). Mean New BEC sur-

face value are lower by 52% in the Southern Ocean and by 36% in the North Pacific relative to the Old BEC, and in each case in good agreement with the field observations. Surface values in the North Atlantic and North Indian oceans are somewhat higher in the New BEC simulation than in the observations or the Old BEC simulation.

Another way to evaluate the model simulations is to examine the binned iron distributions over different depth ranges. Figure 4 compares the binned distributions (bin width 0.05 nM) from our open ocean subset of the observational database with model output that again has been sub-sampled at the same month, depth, and location as the observations. This gives the model output the same sampling biases present in the observational data. The thick line in Fig. 4 represents the observational dataset, the thin line the Old BEC simulation, and the medium thickness line the New BEC simulation. Note the decline in the total number of observations with increasing depth. The observations have a primary peak in the surface distribution at low iron concentrations (<0.2 nM, Fig. 4a). This primary peak is shifted to progressively higher values as depth increases (~0.15–0.35 nM in subsurface, Fig. 4b, and a broader peak in the deep ocean centered on ~0.6–0.7 nM, Fig. 4c). It can be seen at all depth ranges, that the New BEC simulation has binned distributions much closer to the observations than the Old BEC. Both the observations and the New BEC simulation have a strong, low iron peak in surface waters (~0.05–0.2 nM) with a secondary broader peak centered at ~0.7 nM. This higher iron peak is larger in the observations, while both BEC simulations have another peak at iron concentrations >1.2 nM, illustrating the high bias in the BEC model in surface waters. In subsurface waters (103–502 m, Fig. 4b), the low iron peak from the New BEC simulation is in much better agreement with the observations than the Old BEC, but is shifted to slightly higher iron concentrations. In the deeper ocean (>502 m) the Old BEC simulation has a very narrow distribution peaking between 0.45–0.5 nM. The New BEC simulation has a broader distribution also seen in the observations (Fig. 4c). Here the BEC has less values above 0.65 nM than are seen in the observations, illustrating the subsurface, underestimate of high-end iron values.

We compare the spatial patterns of annual mean iron concentration over several

BGD
4, 1279–1327, 2007

depth ranges in Figs. 5–7 for the Old BEC, New BEC, SedOnly, and DustOnly simulations. We focus first on differences between the Old BEC and New BEC simulations. The New BEC simulation has high iron concentrations in surface waters along the continental margins in many regions due to the improved sedimentary source (Fig. 5b). A similar pattern is seen in the observational data in the eastern North and South Pacific, in the southwestern Ross Sea, and south of Australia, nearly everywhere onshore-offshore transects for dissolved iron are available (Fig. 5e). In both the model and the observations these high iron values do not extend far from the continental source regions into the open ocean, depleted by high scavenging rates and biological uptake in surface waters. In the subsurface observations (and in the New BEC simulation) the influence of the continental shelf source can often be seen to extend further offshore (Figs. 6b and e). In particular in the sub-euphotic zone observations in the North Pacific there is a consistent pattern of higher iron concentrations along the margins, decreasing towards the center of the basin (Figs. 6e and 7e).

Another distinct pattern apparent in the observations is the tendency for much higher sub-euphotic zone iron concentrations in the mid-to-high latitude North Pacific than in the open Southern Ocean (Figs. 6e and 7e). This pattern is captured to a large extent in the New BEC simulation, but not in the Old BEC simulation (Figs. 6a–b, 7a–b). In the Old BEC simulation where dissolved iron is mainly driven by dust inputs the North Pacific has iron concentrations only marginally higher than the Southern Ocean. We show in subsequent sections, that it is, in part, the improved sedimentary iron source that allows the New BEC simulation to capture this observed iron distribution pattern. Putting a higher fraction of scavenged iron on the sinking particles is also a factor.

Comparing the New BEC and SedOnly simulations there is an expected drastic decrease in surface iron concentration in the North Atlantic and North Indian oceans without the dust source for iron (Figs. 5b–c). More surprising is the basin-wide decline in surface and subsurface iron concentrations across the Pacific with only sediment (Figs. 5b–7b) or with only dust (Figs. 5c–7c) sources for dissolved iron, indicating that both sources contribute substantially to open ocean iron concentrations. A similar pat-

tern is seen in most other areas outside the high dust deposition areas in the North Atlantic and North Indian oceans. Comparing panels b–d in Figs. 6 and 7, it can be seen that the elevated iron concentrations in the northwest North Pacific are mainly driven by the sedimentary iron source that is mixed and advected offshore, with a lesser contribution from dust deposition. The sedimentary source is also more significant than dust in the eastern tropical Pacific (panels b–d in Figs. 5 and 6).

In several basins, the western boundary currents advect iron from the continental source into the open ocean at high latitudes (panels b and c in Fig. 5–7). This is particularly apparent in the case of the Gulf Stream in the North Atlantic. In the New BEC simulation in the Southern Ocean long plumes of elevated dissolved iron concentration can be seen extending for hundreds to even thousands of kilometers downstream of sediment source regions around New Zealand and in the SW Atlantic sector in the subeuphotic zone waters (Figs. 6b and 7b). The relatively low particle export in the Southern Ocean and consequent weaker scavenging loss allows for advection of dissolved iron far from the source regions. Such long range, rapid transport by the Antarctic Polar Front of sedimentary-derived iron was suggested to account for the high concentrations observed along 6° W in the Southern Ocean (de Baar et al., 1995; Löscher et al., 1997; see Figs. 5e and 6e). Our results support this idea, although iron is more depleted in the simulations by the time it reaches this location (compare Figs. 6c and 6e). Our coarse resolution model does not capture well the narrow current and fast current speed associated with the Antarctic Polar Front, so there is more time for iron removal during transit in the model.

We calculated the basin-scale mean iron concentrations for each of our simulations to further gauge the relative influences of the sedimentary and mineral dust sources for iron (Table 2). Compared with the New BEC simulation, surface iron concentrations in the SedOnly simulation decline by 72% and 60% in the North Atlantic and North Indian oceans, not surprising given the recognized importance of dust deposition in these regions. However, in the DustOnly simulation iron declined by 18% in both the North Atlantic and North Indian oceans, indicating some influence on the basin mean

value even in these high deposition areas. A very strong sedimentary influence was seen in the North Pacific, where mean surface iron concentration declined by 73% in the DustOnly simulation relative to the New BEC simulation (Table 2). Some of this is due to the large decreases (more than an order of magnitude) in the coastal regions, but as illustrated in Fig. 5, open ocean concentrations are also impacted. Removal of the dust source for iron in this region decreases mean iron concentration by 32% in the North Pacific. A similar pattern is seen in the equatorial Pacific where mean iron declined by 82% in surface waters, and 54% in subsurface waters in the DustOnly simulation. The Southern Ocean mean iron concentration also decreased by 43% in surface waters without the sediment source, and by 24% without the dust source for iron (Table 2). In each case there is a contribution towards the mean value from the large, localized reductions along the continental margins, and a contribution from more modest reductions in the open ocean. To distinguish between these margin and open ocean effects, we also computed mean iron concentrations in the open ocean North Pacific (160–220° E and 15–45° N) in these three simulations, with mean iron concentrations of 0.19 nM for the New BEC, 0.075 nM for the SedOnly, and 0.085 nM for the DustOnly simulations. Thus, removing the dust source reduced open ocean iron concentrations by 60%, and removing the sediment source decreased open ocean iron concentrations by 55%. Both sources significantly impact the open ocean iron distributions, with a moderately stronger impact from dust.

We also examined the impacts of each source on globally integrated primary production, export production, and nitrogen fixation by comparing output from the New BEC, SedOnly, and DustOnly simulations. Due to its more diffuse input pattern the removal of the dust source had a stronger impact on these global-scale biogeochemical fluxes (Table 3). Primary production in the SedOnly simulation was reduced by 12% relative to the New BEC simulation, with export production reduced by 15% and nitrogen fixation reduced by 38%. Reductions in the DustOnly simulation were still quite significant, relative to the New BEC simulation, primary production was reduced by 5%, export production by 10%, and nitrogen fixation by 34%. Thus, both sources for dissolved iron

BGD
4, 1279–1327, 2007

contribute substantially in driving productivity and ocean biogeochemical cycles, with a modestly stronger impact from the mineral dust source.

In some respects, these impacts on the carbon cycle do not seem proportional to the drastic declines in mean iron concentrations seen in Table 2. There are very large decreases beneath the main dust plumes and in shallow waters along the continental margins, much of this is "excess" iron that would otherwise be removed by scavenging in these iron-replete regions. Also, because scavenging removal rates of dissolved iron in the model progressively increase at iron concentrations above 0.6 nM, removing either iron source lowers iron concentrations, decreasing scavenging losses for the other source as iron concentrations are reduced in high-iron areas. Even outside these high-iron areas, some of the iron decrease occurs in places where iron is not the nutrient limiting phytoplankton growth rates. Lastly, there is a downstream effect, where reductions in production and export in HNLC regions are partially offset by increases elsewhere due to lateral transport of nutrients (see Dutkiewicz et al., 2005).

In our New BEC simulation each phytoplankton functional group is iron-limited in their growth over about one third of the oceans (Table 3). The spatial patterns vary by group with iron-limitation for the small phytoplankton and diatoms concentrated in the HNLC regions, and iron-limitation for the diazotrophs spread over much of the tropics and subtropics (see Moore et al., 2004). In the SedOnly and DustOnly simulations this iron-limited area increases dramatically to about 60% for each group (Table 1), with much of the increase in the Pacific basin where both sources contribute strongly to open ocean iron distributions.

We compare output from the New BEC simulation with the LowFe, NoDesorp, and HighDesorp sensitivity simulations in Figs. 8–10. It can be seen that the inclusion of an explicit desorption of iron from sinking particles has little effect in surface waters, increasing dissolved iron concentrations by a few percent in most regions (Fig. 8, panels a, b, and d, Table 2). This is because the release of iron is quite small relative to the forward scavenging rate onto particles. The similarity in surface iron concentrations leads to similar global biogeochemical fluxes in these simulations (Table 3). In partic-

ular, the HighDesorp simulation has nearly identical rates of nitrogen fixation, primary and export production (Table 3), and fits the surface iron observations essentially as well as the New BEC simulation (not shown).

Deeper in the ocean where particle scavenging is reduced, including desorption increases iron concentrations significantly in some regions (by 29% in the deep North Pacific and Southern Ocean, see Table 2, compare panels a and b in Figs. 9 and 10). Deep ocean concentrations are further increased in these regions in the HighDesorp case (modified by the higher base scavenging rate in this simulation). In deep ocean areas where iron concentrations exceeds 0.6 nM, desorption has less effect due to the high scavenging rates. Thus, these three simulations have similar deep ocean concentrations in the deep North Atlantic and North Indian oceans (Fig. 10, panels a, b, and d).

Comparing the New BEC simulation and the LowFe simulation, both simulations have similar, low concentrations in the lower latitude surface waters, away from the high dust deposition regions (Fig. 8, panels a and c). In the subsurface waters though, the LowFe simulations has very high iron concentrations (>0.5 nM in most regions), well above the observed values (Fig. 9, panels a, c, and e). Even with the very low (minimal) iron inputs in this simulation, subsurface iron concentrations are grossly overestimated without substantial removal of iron by scavenging where iron <0.6 nM. This elevated subsurface iron strongly impacts surface waters in regions of deeper winter mixing and upwelling, as in the Southern Ocean and eastern equatorial Pacific (Fig. 8c). Averaged over the equatorial Pacific, surface concentrations in the LowFe simulation are slightly lower in than in the New BEC simulation (0.14 nM vs. 0.16 nM), but are more than twice the New BEC values in subsurface waters (Table 2). Similarly, in the Southern Ocean the subsurface LowFe iron concentrations are more than double the New BEC values, and much higher than the observations (Tables 1 and 2, Fig. 9). Thus, surface iron fields can be misleading as biological drawdown keeps iron at reasonable concentrations, even when the inputs from subsurface waters are much too high. In the deep ocean, the LowFe simulations are slightly above 0.6 nM beneath the major

BGD
4, 1279–1327, 2007

dust plumes, and slightly below 0.6 nM elsewhere, again with a poor match to the observed iron distributions (Fig. 10, panels c and e, Table 2). The New BEC simulation is in broad agreement with the observations in the North Pacific ocean at shallow and mid-water depths (Figs. 5–7, panels b and e). However, in the deep ocean the model underestimates the observed concentrations in this region, even in the HighDesorp simulation (Fig. 10). Further increasing the desorption rate could increase deep North Pacific simulated values, but would also push other regions, like the Southern Ocean to values well above the observations. It is likely that iron inputs to the North Pacific are underestimated. This could be due to our low surface solubility for mineral dust iron (2%), or perhaps the flux from the continental margins to the open ocean, though substantial, is still underestimated in this region.

4 Discussion

The results presented here indicate a strong influence of the continental margin iron source on both the basin mean and open ocean iron concentrations, and on biological productivity, nitrogen fixation, and the export of organic matter. Inputs from mineral dust deposition had a modestly stronger impact on open ocean iron concentrations and biogeochemical cycling, but the sedimentary source was significant in all regions, except perhaps beneath the strongest dust plumes in the North Atlantic and northern Indian Oceans. Ocean biogeochemical models need to include the sedimentary source for iron, as suggested by Elrod et al. (2004). Models without this source will seriously overestimate the biogeochemical sensitivity to variations in dust deposition to the oceans. The combination of high particle scavenging and biological uptake largely remove the high-iron, continental signal close to the coasts in surface waters, but in subsurface waters, where losses are reduced, this continental signal can travel far from the margin source areas.

There is still considerable uncertainty in the strength of both major sources for dissolved iron. There are very few observations of dust deposition to constrain the at-

mospheric transport models. Similarly, a number of recent studies suggest that our constant surface solubility for the iron in mineral dust of 2% (or the 1% often used in other studies) could be low by an order of magnitude in many regions (i.e., see Luo et al., 2005; and references therein, also Sedwick et al., 2005; Fan et al., 2006; Bakker et al., 2006). Thus, our simulations may significantly underestimate dissolved iron inputs to surface waters from mineral dust. One uncertainty in our sedimentary source is missing offshore transport in the model due to eddies and other mesoscale physical processes ,which likely play an important role (Johnson et al., 2005; Lam et al., 2006). Similarly, the model advects only dissolved iron offshore, when small particulates likely also contribute (Lam et al., 2006). The model likely significantly underestimates the local scavenging loss of this iron near the source regions, as often the flux from a small area (a few % of our grid box) is instantly diluted throughout the model grid cell, resulting in much lower concentrations than would happen in a finer resolution model (or in situ). Our results are also extrapolating from a relatively small set of observations (Elrod et al., 2004) and use model estimates of the organic carbon flux to the sediments (likely too low) to drive the sedimentary release of iron.

Our inclusion of an explicit desorption of iron from sinking particles improved the fit to observations in the deeper ocean (increasing deep ocean concentrations by up to 29% in some regions), but had little impact on surface iron concentrations and upper ocean biogeochemical cycling. This is similar to the pattern suggested for ^{234}Th with desorption generally negligible in surface waters, where high particle concentrations lead to strong scavenging removal (i.e., Bruland and Lohan, 2004). In local and upper ocean models, desorption of iron could likely be ignored in favor of a net scavenging rate onto particles.

Our parameterization for increasing scavenging rates where dissolved iron concentration exceeds 0.6 nM led the model to overestimate high-end iron concentrations in surface waters and to underestimate the high-end values in subsurface waters. The optimum value of the coefficient Chigh, used in this parameterization, was several-fold higher for surface waters than for subsurface waters. Several factors may drive these

results. Iron inputs to surface waters in the high dust deposition regions may be overestimated, as values below our assumed 2% solubility have been observed for fresh Saharan dust (i.e., Baker et al., 2006). In these high-scavenging regions, the scavenging efficiency may decrease with depth as organic coatings on sinking particles are degraded, or as likely sites on the particles for binding iron are filled up.

Our results suggest that relatively strong scavenging removal of iron from subsurface waters is required to match the observations of dissolved iron. This was true in our simulations with relatively high iron inputs (including the sedimentary source and some subsurface release from dust particles), and was also apparent in the sensitivity experiment with a low-end estimate of iron inputs (LowFe, constant 1% dissolution from mineral dust). In most regions, the dissolved iron concentrations are well below 0.6 nM in these subsurface waters, and, thus, nearly all the dissolved iron would be bound to organic ligands (i.e., Rue and Bruland, 1995; 1997; van den Berg, 1995; Wu and Luther, 1995). Therefore, much of this scavenging removal is likely due to aggregation followed by removal on sinking particles of the colloidal ligand-bound iron (Wu et al., 2001; Nishioka et al., 2001; de Baar and de Jong, 2001). Models that explicitly include the ligand and aggregation dynamics would be computationally expensive, but could potentially improve simulations of the marine iron cycle. The parameterization of these processes in the New BEC simulation provides a reasonable fit to the observed iron concentrations, particularly for the subsurface waters (Fig. 3d and Fig. 6 panels b and e). Relatively high scavenging rates are required to match the observed iron distributions. The residence times for dissolved iron over different depth ranges are summarized in Table 4. Areas with high inputs of iron (where dissolved concentrations exceed 0.6 nM) have shorter residence times due to higher scavenging rates. Upper ocean residence times are quite short, 1.3 and 4.2 years for the upper 103 m and upper 502 m away from the high iron regions. In the highest dust input regions beneath the major plumes residence times are only a month or two.

The deep ocean residence time away from the high iron regions was 35 years, somewhat less than the estimate of 70–140 years by Bruland et al. (1994) for the deep North

Pacific. De Baar and de Jong (2001) estimated surface ocean residence time of a few months, and for the deep ocean of 15–41 years, assuming a sedimentary input equal to inputs from dust deposition. Thus, our model results which include both sources are of similar magnitude (Table 4). Parekh et al. (2005) estimated mean ocean residence time of 233 years, in a simulation with a 1% surface dissolution of mineral dust as the only source. The higher iron inputs in our simulation require stronger scavenging removal and shorter residence times to maintain realistic iron concentrations. Bergquist and Boyle (2006) estimated a longer scavenging residence time of 270 years based on differences in deep ocean measurements of dissolved iron at North Atlantic and South Atlantic sites, the estimated transit time between the two sites, and an estimated input of dissolved iron from sinking biogenic particles. This estimate assumed an iron to carbon ratio equivalent of 10 μmol/mol in estimating inputs from biogenic particles. This estimate is reasonable for biogenic particles produced in the surface ocean, but the particles releasing iron in the deep ocean would likely have considerably higher iron content due to scavenging of dissolved iron through the water column (perhaps as much as 1–2 orders of magnitude higher Fe/C ratios, lithogenic particles also likely scavenge iron and release some of it in the deep ocean). Increased iron inputs would significantly increase the estimated scavenging loss for iron, and reduce the estimated residence time. Our estimates of dissolved iron inputs to the oceans and model results suggest a short mean global residence time for iron of a few decades at most, in agreement with the estimate of de Baar and de Jong (2001).

In the surface ocean (<103 m) there is a bimodal distribution in the observed iron distributions, with a larger peak centered at ~0.1–0.15 nM and a secondary broad peak centered at ~0.6–0.8 nM (Fig. 4a). The high-end iron peak reflects samples mainly from the high deposition regions, or samples from other areas taken shortly after dust deposition events. Dust deposition likely varies considerably even within the high deposition regions, but it seems there is a strong tendency for iron above this peak to be rapidly removed by scavenging. There is a similar high-end peak in the observations in the deep ocean (Fig. 4c), suggesting a common controlling process, most likely in-

BGD
4, 1279–1327, 2007

creased scavenging losses as iron exceeds ~0.6–0.7 nM, as suggested by Johnson et al. (1997a).

The surface peak in the observations between ~0.1–0.15 nM in surface waters is a function of removal by particle scavenging and biological uptake of dissolved iron. This peak in the distribution represents waters that receive a considerable range in iron inputs from the sediments and atmospheric dust deposition – from very low inputs to the equatorial Pacific and Southern Ocean, to moderate levels of input in the higher latitude North Pacific (Zender et al., 2003; Luo et al., 2003; see also MBa this issue). The combination of particle scavenging and biological uptake appear to deplete surface iron concentrations down to relatively low, constant levels, despite the variations in iron inputs from dust deposition and laterally from the continental margins. Several factors likely play a role in this pattern. In some regions, increased iron inputs will lead to higher biological production and export, providing more particles to scavenge and remove dissolved iron. When iron is more plentiful, phytoplankton Fe/C ratios will be higher, in part due to luxury uptake by larger diatoms, removing iron more efficiently (i.e., Sunda and Huntsman, 1997). Conversely, the number of binned samples declines sharply in our lowest bin (0.0–0.05 nM). As iron falls to very low concentrations (<0.1 nM), the phytoplankton will adapt by lowering their Fe/C ratios, thus decreasing the export efficiency. Also, biological uptake will be reduced as ambient iron concentration approaches or even falls below the half-saturation Fe uptake values. Fitzwater et al. (1996) estimated a community value of 0.12 nM in the diatom-dominated IronEx bloom in the equatorial Pacific. Price et al. (1994) estimated ambient community values of 0.035 nM in the equatorial Pacific and 0.22 nM in the subtropical Pacific. Kudo et al. (2006) estimated values of 0.10 nM and 0.08 nM for the micro and nano-sized phytoplankton fractions in the NW subarctic Pacific. Lastly, extreme iron limitation will reduce the formation of biological particles available to scavenge and remove dissolved iron. Less dissolved iron may be in the colloidal size fraction when iron concentrations fall to very low values (Nishioka et al., 2001, 2005). Thus as iron falls to very low concentrations, both the scavenging loss and biological uptake will be reduced.

BGD
4, 1279–1327, 2007

It is important for ocean biogeochemical models that include the marine iron cycle to utilize more fully the growing global database of dissolved iron observations to evaluate and constrain model output. A key metric is the model's ability to reproduce the sub-euphotic zone observed iron concentrations, as inputs from these source waters drive much of the biogeochemical cycling in the oceans. Models that overestimate the subsurface iron pools will underestimate the potential impacts from variations in mineral dust deposition. Although still a limited dataset, the currently available observations can test the large-scale iron distributions from ocean models (MBa and this paper). The available observational data will increase rapidly over the next decade through ongoing research projects and the surveys associated with the CLIVAR and GEOTRACES programs. The growing global database of iron observations will provide new opportunities to improve our understanding of the marine iron cycle.

Acknowledgements. We would like to thank all the researchers, technicians, and students who made the iron measurements and made the data publicly available. Also thanks to P. Parekh, M. Follows, and E. Boyle for publishing their iron observations compilation. This work is funded by a National Science Foundation grant (NSF OCE-0452972 to J. K. Moore) and the UCI Research Experience for Undergraduates (REU) program funded by the National Science Foundation (NSF ATM-0453295 to J. K. Moore).

References

Archer, D. E. and Johnson, K.: A model of the iron cycle in the ocean, Global Biogeochem. Cycles, 14, 269–279, 2000.

Armstrong, R. A., Lee, C., Hedges, J. I., Honjo, S., and Wakeham, S. G.: A new, mechanistic model for organic carbon fluxes in the ocean based on the quantitative association of POC with ballast minerals, Deep-Sea Res. II, 49, 219–236, 2002.

Aumont, O., Maier-Reimer, E., Blain, S., and Monfray, P.: An ecosystem model of the global ocean including Fe, Si, P co-limitations, Global Biogeochem. Cycles, 17, 1060, doi:10.1029/2001GB001745, 2003.

Bacon, M. P. and Anderson, R. F.: Distribution of Thorium isotopes between dissolved and particulate forms in the deep sea, J. Geophys. Res., 87, 2045–2056, 1982.
Bakker, A. R., Jickells, T. D., Witt, M., and Linge, K. L.: Trends in the solubility of iron, aluminum, manganese and phosphorus in aerosol collected over the Atlantic Ocean, Mar. Chem., 98, 43–58, 2006.
Berelson, W., McManus, J., Coale, K., Johnson, K., Burdige, D., Kilgore, T., Colodner, D., Chavez, F., Kudela, R., and Boucher, J.: A time series of benthic flux measurements from Monterey Bay, CA., Continental Shelf Res., 23, 457–481, 2003.
Berelson, W., McManus, J., Coale, K., Johnson, K., Burdige, D., Kilgore, T., Burdige, T., and Pilskaln, C.: Biogenic matter diagenesis on the sea floor: a comparison between two continental margin transects, J. Mar. Res., 54, 731–762, 1996.
Bergquist, B. A. and Boyle, E. A.: Dissolved iron in the tropical and subtropical Atlantic Ocean, Global Biogeochem. Cycles, 20, GB1015, doi:10.1029/2005GB002505, 2006.
Berman-Frank, I., Cullen, J. T., Shaked, Y., Sherrell, R. M., and Falkowski, P. G.: Iron availability, cellular iron quotas, and N fixation in Trichodesmium, Limnol. Oceanogr., 46, 1249–1260, 2001.
Blain, S., Treguer, P., Belviso, S., Bucciarelli, E., Denis, M., Desbre, S., Fiala, M., Jezequel, V. M., LeFevre, J., Mayzaud, P., Marty, J., and Razouls, S.: A biogeochemical study of the island mass effect in the context of the iron hypothesis: Kerguelen Islands, Southern Ocean, Deep-Sea Res. I, 48, 163–187, 2001.
Boyd, P. W., Watson, A. J., Law, C. S., Abraham, E. R., Trull, T., Murdoch, R., Bakker, C. E., Bowei, A. R., Buesseler, K. O., Chang, H., Charette, M., Croot, P., Downing, K., Frew, R., Gall, M., Hadfield, M., Hall, J., Harvey, M., Jameson, G., LaRoche, J., Liddicoat, M., Ling, R., Maldonado, M.T ., McKay, R. M., Nodder, S., Pickmere, S., Pridmore, Rintoul, S., Safi, K., Sutton, P., Strzepek, R., Tanneberger, K., Turner, S., Waite, A., and Zeldis, J.: A mesoscale phytoplankton bloom in the polar Southern Ocean stimulated by iron fertilization, Nature, 407, 695–702, 2000.
Bruland, K. W., Orians, K. J., and Cowen, J. P.: Reactive trace metals in the stratified central North Pacific, Geochimica et Cosmocimica Acta, 58, 3171–3182, 1994.
Bruland, K. W. and Lohan, M. C.: The control of trace metals in seawater. Chapter 2 in The Oceans and Marine Geochemistry, Vol. 6 (Ed. Elderfield, H.) in Treatise on Geochemistry, edited by: Holland, H. D. and Turekian, K. K., 2004.
Bruland, K. W., Rue, E. L., Smith, G. J., and DiTullio, G. R.: Iron, macronutrients and diatom

blooms in the Peru upwelling regime : brown and blue waters of Peru, Mar. Chem., 93, 81–103, 2005.
Burd, A. B., Jackson, G. A., and Moran, S. B.: A coupled adsorption-aggregation model for the POC/^{234}Th ratio of marine particles, Deep-Sea Res. I., 47, 103–120, 2000.
Chase, Z., Johnson, K. S., Elrod, V. A., Plant, J. N., Fitzwater, S. E., Pickell, L., and Sakamoto, C. M. : Manganese and iron distributions off central California influenced by upwelling and shelf width, Mar. Chem., 95, 235–254, 2005.
Christian, J. R., Verschell, M. A., Murtugudde, R., Busalacchi, A. J., and McClain, C. R.: Biogeochemical modeling of the tropical Pacific Ocean II. Iron biogeochemistry, Deep-Sea Res. II, 49, 545–565, 2002.
Coale, K. H., Johnson, K. S., Fitzwater, S. E., Gordon, R. M., Tanner, S., Chavez, F. P., Ferioli, L., Sakamoto, C., Rogers, P., Millero, F., Steinberg, P., Nightingale, P., Cooper, D., Cochlan, W. P., Landry, M. R., Constantiou, J., Rollwagen, G., Trasvina, A., and Kudela, R.: A massive phytoplankton bloom induced by an ecosystem-scale iron fertilization experiment in the equatorial Pacific Ocean, Nature, 383, 495–501, 1996.
Coale, K. H., Johnson, K. S., Chavez, F. P., Buesseler, K. O., Barber, R. T., et al.: Southern Ocean Iron Enrichment Experiment: Carbon cycling in high- and low-Si waters, Science, 304, 408–414, 2004.
Coale, K. H., Wang, X., Tanner, S. J., and Johnson, K. S. : Phytoplankton growth and biological response to iron and zinc addition in the Ross Sea and Antarctic Circumpolar Current along 170° W, Deep-Sea Res. II, 50, 635–653, 2003.
Collins, W. D., Blackmon, M., Bitz, C. M., Bonan, G. B., Bretherton, C. S., Carton, J. A., Chang, P., Doney, S., Hack, J. J., Kiehl, J. T., Henderson, T., Large, W. G., McKenna, D., and B. D., and Santer, S. D.: The Community Climate System Model: CCSM3, J. Climate, 19, 2122–2143, 2006.
Conkright, M. E., Locarnini, R. A., Garcia, H. E., O'Brien, T. D., Boyer, T. P., Stevens, C., and Antonov, J. I.: World Ocean Atlas 2001: Objective analysis, data statistics, and figures, CD ROM documentation. National Oceanographic Data Center, Silver Spring, MD, 2002.
Cullen, J. T., Bergquist, B. A., and Moffett, J. W. : Thermodynamic characterization of the partitioning of iron between soluble and colloidal species in the Atlantic Ocean, Mar. Chem., 98, 295–303, 2006.
de Barr, J. W. H., Boyd, P. W., Coale, K. H., Landry M. R., Tsuda, A., Assmy, P., Bakker, D. C. E., Boze, Y., Barber, R. T., Brzezinski, M. A., Buesseler, K. O., Boyé, M., Croot, P. L.,

Gervais, F., Gorbunov, M. Y., Harrison, P. J., Hiscock, W. T., Laan, P., Lancelot, C., Law, C. S., Levasseur, M., Marchetti, A., Millero, F. J., Nishioka, J., Nojiri, Y., van Oijen, T., Riebesell, U., Rijkenberg, M. J. A., Saito, H., Takeda, S., Timmermans, K. R., Veldhuis, M. J. W., Waite, A. M., and Wong, C. S.: Synthesis of iron fertilization experiments: From the Iron age in the Age of Enlightenment, J. Geophys. Res., 110, C09S16, doi:10.1029/2004JC002601, 2005.

de Baar, H. J. W. and De Jong, J. T. M.: Distributions, sources and sinks of iron in seawater. In: Turner, D. and Hunter, K.A. (Eds.) Biogeochemistry of Iron in Seawater, IUPAC Book Series on Analytical and Physical Chemistry of Environmental Systems, 7, 123–253, 2001.

de Baar, H. J. W., de Jong, J. T. M., Nolting, R. F., Timmermans, K. R., van Leeuwe, M. A., Bathmann, U., Rutgers van der Loeff, M., and Sildam, J.: Low dissolved Fe and the absence of diatom blooms in remote Pacific waters of the Southern Ocean, Mar. Chem., 66, 1–34, 1999.

Doney, S. C. and Ducklow, H. W.: A decade of synthesis and modeling in the US Joint Global Flux Study, Deep-Sea Res. II, 53, 451–458, 2006.

Doney, S. C., Lindsay, K., Fung, I., and John, J.: Variability in a stable, 1000-yr coupled climate-carbon simulation, J. Climate, 19, 3033–3054, 2006.

Dutkiewicz, S., Follows, M., and Parekh, P.: Interactions of the iron and phosphorus cycles: A three-dimensional model study, Global Biogeochem. Cycles, 19, GB1021, doi:10.1029/2004GB002342, 2005.

Elrod, V. A., Berelson, W. M., Coale, K. H., and Johnson, K. S.: The flux of iron from continental shelf sediments: A missing source of global budgets, Geophys. Res. Lett., 31, L12307, doi:10.1029/2004GL020216, 2004.

Falkowski, P. G.: Evolution of the nitrogen cycle and its influence on the biological sequestration of CO2 in the ocean, Nature, 387, 272–275, 1997.

Fan, S. M., Moxim, W. J., and Levy II, H.: Aeolian input of bioavailable iron to the ocean. Geophys. Res. Lett., 33, L07602, doi:10.1029/2005GL024852, 2006.

Fitzwater, S. E., Coale, K. H., Gordon, R. M., Johnson, K. S., and Ondrusek, M. E.: Iron deficiency and phytoplankton growth in the equatorial Pacific. Deep-Sea Res. II, 43, 995–1015, 1996.

Frew, R. D., Hutchins, D. A., Nodder, S., Sanudo-Wilhelmy, S., Tovar-Sanchez, A., Leblanc, K., Hare, C. E., and Boyd, P. W.: Particulate iron dynamics during FeCycle in sub-antarctic waters southeast of New Zealand, Global Biogeochem. Cycles, 20, GB1S93, doi:10.1029/2005GB002558, 2006.

Fung, I. Y., Meyn, S. K., Tegen, I., Doney, S. C., John, J. G., and Bishop, J. K. B.: Iron supply and demand in the upper ocean, Global Biogeochem. Cycles, 14, 281–295, 2000.
Gregg, W., Ginoux, P., Schopf, P. S., and Casey, N. W.: Phytoplankton and iron: validation of a global three-dimensional ocean biogeochemical model, Deep-Sea Res. II, 50, 3143–3169, 2003.
Gruber, N.: The dynamics of the marine nitrogen cycle and its influence on atmospheric CO_2 variations, In: The Ocean Carbon Cycle, Eds. Follows, M., Oguz, T., Kluwer Academic Publishers, Netherlands, 97–148, 2004.
Guo, L., Hung, C. C., Santschi, P. H., and Walsh, I. D.: ^{234}Th scavenging and its relationship to acid polysaccharide abundance in the Gulf of Mexico, Mar. Chem., 78, 103–119, 2002.
Honeyman, B. D., Balistrieri, L. S., and Murray, J. W.: Oceanic trace metal scavenging: the importance of particle concentration, Deep-Sea Res., 35, 227–246, 1988.
Jickells, T. D., An, Z. S., Anderson, K. K., Baker, A. R., Bergametti, G., et al.: Global iron connections between desert dust, ocean biogeochemistry, and climate, Science, 308, 67–71, 2005.
Johnson, K., Gordon, M. R, and Coale, K. H.: What controls dissolved iron concentrations in the world ocean?, Mar. Chem., 57, 137–161, 1997a.
Johnson, K., Gordon, M. R, and Coale, K. H.: What controls dissolved iron concentrations in the world ocean? – Authors closing comments, Mar. Chem., 57, 181–186, 1997b.
Johnson, K. S., Chavez, F. P., and Friederich, G. E.: Continental-shelf sediment as a primary source of iron for coastal phytoplankton, Nature, 398, 697–700, 1999.
Johnson, K. S., Elrod, V. A., Fitzwater, S. E., Plant, J. N., Chavez, F. P., Tanner, S. J., Gordon, R. M., Westphal, D. L., Perry, K. D., Wu, J., and Karl, D. M.: Surface ocean-lower atmosphere interactions in the Northeast Pacific Ocean Gyre: Aerosols, iron, and the ecosystem response, Global Biogeochem. Cycles, 17, 1063, doi:10.1029/2002GB002004, 2003.
Johnson, W. K., Miller, L. A., Sutherland, N. D., and Wong, C. S.: Iron transport by mesoscale Haida eddies in the Gulf of Alaska, Deep-Sea Res. II, 52, 933–953, 2005.
Klaas, C. and Archer, D. E.: Association of sinking organic matter with various types of mineral ballast in the deep sea: Implications for the rain ratio, Global Biogeochem. Cycles, 16, 1116, doi:10.1029/2001GB001765, 2002.
Kudo, I., Noiri, Y., Nishioka, J., Taira, Y., Kiyosawa, H., and Tsuda, A.: Phytoplankton community response to Fe and temperature gradients in the NE (SERIES) and NW (SEEDS) subarctic Pacific Ocean, Deep-Sea Res. II, 53, 2201–2213, 2006.

Lam, P. J., Bishop, J. K. B., Henning, C. C., Marcus, M. A., Waychunas, G. A., and Fung, I. Y.: Wintertime phytoplankton bloom in the subarctic Pacific supported by continental margin iron, Global Biogeochem. Cycles, 20, GB1006, doi:10.1029/2005GB002557, 2006.

Large, W. G. and Yeager, S. G.: Diurnal to decadal global forcing for ocean and sea-ice models: the data sets and flux climatologies. NCAR Technical Note NCAR/TN-460+STR, 111 pp, 2004.

Le Quéré, C., S. P. Harrison, I. C. Prentice, E. T. Buitenhuis, O. Aumont, et al.: Ecosystem dynamics based on plankton functional types for global ocean biogeochemistry models, Global Change Biol., 11, 2016–2040, 2005.

Löscher, B. M., de Baar, H. J. W., de Jong, J. T. M.,and Goeyens, L.: The distribution of Fe in the Antarctic Circumpolar Current, Deep Sea-Res. II., 143–187, 1997.

Luo, C., Mahowald, N., and del Corral, J.: Sensitivity study of meteorological parameters on mineral aerosol mobilization, transport and distribution, J. Geophys. Res., 108(D15), 4447, doi:10.1029/2003JD0003483, 2003.

Luo, C., Mahowald, N. M., Meskidze, N., Chen, Y., Siefert, R. L., Baker, A. R., and Johansen, A. M.: Estimation of iron solubility from observations and a global aerosol model, J. Geophys. Res., 110, D23307, doi:10.1029/2005D006059, 2005.

Luther III, G. W. and Wu, J.: What controls dissolved iron concentrations in the world ocean? – a comment., Mar. Chem., 57, 173–179, 1997.

Mackey, D. J., O'Sullivan, J. E., and Watson, R. J.: Iron in the western Pacific: a riverine or hydrothermal source for iron in the Equatorial Undercurrent?, Deep-Sea Res. I, 49, 877–893, 2002.

Mahowald, N. M., Baker, A. R., Bergametti, G., Brooks, N., Duce, A., Jickells, T. D., Kubliay, N., Prospero, J. M., and Tegen, I.: Atmospheric global dust cycle and iron inputs to the ocean, Global Biogeochem. Cycles, 19, GB4025, doi:10.1029/2004GB002402, 2005.

Mahowald, N. M., Muhs, D. R., Levis, S., Rasch, P. J., Yoshioka, M., Zender, C. S., and Luo, C.: Change in atmospheric mineral aerosols in response to climate: Last glacial period, preindustrial, modern, and doubled carbon dioxide climates, J. Geophys. Res., 111, D10202, doi:10.1029/2005JD006653, 2006.

Martin, J. H., Gordon, R. M., and Fitzwater, S. E.: The case for iron, Limnol. Oceanogr., 36, 1793–1802, 1991.

Michaels, A. F., Karl, D. M., and Capone, D. G.: Elemental stoichiometry, new production, and N fixation, Oceanography, 14(4), 68–77, 2001.

Moore, J. K. and Abbott, M. R.: Phytoplankton chlorophyll distributions and primary production in the Southern Ocean, J. Geophys. Res, 105, 28 709–28 722, 2000.
Moore, J. K., Doney, S. C., Kleypas, J. C., Glover, D. M., and Fung, I. Y.: An intermediate complexity marine ecosystem model for the global domain, Deep-Sea Res. II, 49, 403–462, 2002.
Moore, J. K., Doney, S. C., and Lindsay, K.: Upper ocean ecosystem dynamics and iron cycling in a global three-dimensional model, Global Biogeochem. Cycles, 18, GB4028, doi:10.1029/2004GB002220, 2004.
Moore, J. K., Doney, S. C., Lindsay, K., Mahowald, N., and Michaels, A. F.: N fixation amplifies the ocean biogeochemical response to decadal timescale variations in mineral dust deposition, Tellus B, 58B, 560–572, 2006.
Moore, J. K. and Doney S. C.: Iron availability limits the ocean nitrogen inventory stabilizing feedbacks between marine denitrification and nitrogen fixation, Global Biogeochem. Cycles, 21, GB2001, doi:10.1029/2006GB002762, 2007.
Moore J. K. and Braucher, O.: Observations of dissolved iron concentration in the world ocean: Implications and constraints for ocean biogeochemical models, Biogeosci. Discuss., 4, 1241–1277, 2007.
Nishioka, J., Takeda, S., Wong, C. S., and Johnson, W. K.: Size-fractionated iron concentrations in the northeast Pacific Ocean: distribution of soluble and colloidal iron, Mar. Chem., 74, 157–179, 2001.
Nishioka, J., Takeda, S., de Baar, H. J. W., Croot, P. L., Boye, M., Laan, P., and Timmermans, K. R.: Changes in the concentration of iron in different size fractions during an iron fertilization experiment in the open Southern Ocean, Mar. Chem., 95, 51–63, 2005.
Parekh, P., Follows, M. J, and Boyle, E. A.: Modeling the global ocean iron cycle, Global Biogeochem. Cycles, 18, GB1002, doi:10.1029/2003GB002061, 2004.
Parekh, P., Follows, M. J., and Boyle, E. A.: Decoupling of iron and phosphate in the global ocean, Global Biogeochem. Cycles, 19, GB2020, doi:10.1029/2004GB002280, 2005.
Passow, U., Dunne, J., Murray, J. W., Balistrieri, L., and Alldredge, A. L.: Organic carbon to ^{234}Th ratios of marine organic matter, Mar. Chem., 100, 323–336, 2006.
Price, N. M., Ahner, B. A., and Morel, F. M. M.: The equatorial Pacific Ocean: Grazer-controlled phytoplankton populations in an iron-limited system, Limnol. Oceanogr., 39, 520–534, 1994.
Reddy, T.E., and Arrigo, K.R.: Constraints on the extent of the Ross Sea phytoplankton bloom. J. Geophys. Res., 111, C07005, doi:10.1029/2005JC003339, 2006.

Rue, E. and Bruland, K.: Complexation of iron (III) by natural organic ligands in the central North Pacific as determined by a new competitive ligand equilibration/adsorptive cathodic stripping voltammetric method, Mar. Chem., 50, 117–138, 1995.

Rue, E. and Bruland, K.: The role of organic complexation on ambient iron chemistry in the equatorial Pacific Ocean and the response of a mesoscale iron addition experiment, Limnol. Oceanogr., 42, 901–910, 1997.

Santschi, P. H., Murray, J. W., Baskaran, M., Benitez-Nelson, C. R., Guo, L. D., Hung, C. C., Lamborg, C., Moran, S. B., Passow, U., and Roy-Barman, M.: Thorium speciation in seawater, Mar. Chem., 100, 250–268, 2006.

Savoye, N., Benitez-Nelson, C., Burd, A. B., Cochran, J. K., Charette, M., Buesseler, K. O., Jackson, G. A., Roy-Barman, M., Schmidt, S., and Elskens, M.: ^{234}Th sorption and export models in the water column: A review, Mar. Chem., 100, 234–249, 2006.

Sedwick, P. N., Church, T. M., Bowie, A. R., Marsay, C. M., Ussher, S. J., Achilles, K. M., Lethaby, P. J., Johnson, R. J., Sarin, M. M., and McGillicuddy, D. J.: Iron in the Sargasso Sea (Bermuda Atlantic Time-series Study region) during summer: Eolian imprint, spatiotemporal variability, and ecological implications. Global Biogeochem. Cycles, 19, GB4006, doi:10.1029/2004GB002445, 2005.

Sunda, W. G. and Huntsman, S. A.: Interrelated influence of iron, light, and cell size on marine phytoplankton growth, Nature, 390, 389–392, 1997.

Timmermans, K. R., van der Wagt, B., and de Baar, H. J. W.: Growth rates, half saturation constants, and silicate, nitrate, and phosphate depletion in relation to iron availability of four large open ocean diatoms from the Southern Ocean, Limnol. Oceanogr., 46, 260–266, 2004.

Tsuda, A., Takeda, H., Saito, H., Nishioka, J., Nojiri, Y., et al.: A mesoscale iron enrichment in the western Subarctic Pacific induces a large centric diatom bloom, Science, 300, 958–961, 2003.

U.S. Department of Commerce: 2-minute global gridded relief data. National Oceanographic and Atmospheric Administration, National Geophysical Data Center, 2006.

van den Berg, C.: Evidence for organic complexation of iron in seawater, Mar. Chem., 50, 139–157, 1995.

Wells, M. L. and Goldberg, E. D.: Colloid aggregation in seawater, Mar. Chem., 41, 353–358, 1993.

Wen, L. S., Jiann, K. T., and Santschi, P. H.: Physicochemical speciation of bioactive metals (Cd, Cu, Fe, Ni) in the oligotrophic South China Sea, Mar. Chem., 101, 104–129, 2006

Wu, J., Boyle, E., Sunda, W., and Wen, L. S.: Soluble and colloidal iron in the oligotrophic North Atlantic and North Pacific, Science, 293, 847–849, 2001.

Wu, J. and Boyle, E.: Iron in the Sargasso Sea: Implications for the processes controlling dissolved Fe distribution in the ocean, Global Biogeochem. Cycles, 16(4), 1086, doi:10.1029/2001GB001453, 2002.

Wu, J. and Luther, G.: Complexation of Fe(III) by natural organic ligands in the Northwest Atlantic Ocean by a competitive ligand equilibration method and kinetic approach, Mar. Chem., 50, 159–177, 1995.

Yeager, S. G., Large, W. G., Hack, J. J., and Shields, C. A.: The Low Resolution CCSM3, J. Climate, 17, 2545–2566, 2006.

Zender, C. S., Bian, H., and Newman, D.: The Mineral Dust Entrainment And Deposition (DEAD) model: Description and 1990s dust climatology, J. Geophys. Res., 108(D14), 4416, doi:10.1029/2002JD002775, 2003.

Table 1. Mean dissolved iron concentrations (nM) in different ocean basins from the observations (O = open ocean subset and A = all observations) and from the Old and New BEC simulated mean iron fields, where the model output has been sub-sampled at the month, depth and location of the field observations. In the Pacific we compute an equatorial mean (from 15° S–15° N) a North Pacific mean (>15° N), and a South Pacific mean (>15° S) Basins and depths not shown had less than 20 observations, surface waters always had >200 observations per basin.

Region and Depth	Oobs	Oold	Onew	Aobs	Aold	Anew
North Indian						
0–103 m	0.99	1.34	1.58	1.21	1.26	1.54
103–502 m	1.43	0.88	1.12	1.50	0.89	1.12
North Atlantic						
0–103 m	0.72	0.96	1.01	0.68	0.97	1.06
103–502 m	0.60	0.59	0.62	0.61	0.59	0.63
502–945 m	0.78	0.60	0.64	0.76	0.60	0.64
>945 m	0.73	0.60	0.63	0.76	0.57	0.62
South Atlantic						
0–103 m	0.45	0.59	0.63	0.44	0.57	0.58
North Pacific						
0–103 m	0.20	0.28	0.18	0.31	0.25	0.27
103–502 m	0.40	0.41	0.47	0.69	0.40	0.50
502–945 m	0.67	0.47	0.52	0.84	0.45	0.54
>945 m	0.77	0.49	0.45	0.89	0.48	0.47
Equatorial Pacific						
0–103 m	0.11	0.14	0.091	0.84	0.11	0.30
103–502 m	0.29	0.26	0.20	0.98	0.25	0.22
>945 m	0.64	0.40	0.38	1.10	0.40	0.37
South Pacific						
0–103 m	–	–	–	0.31	0.085	0.22
Southern Ocean						
0–103 m	0.17	0.31	0.15	0.50	0.31	0.21
103–502 m	0.23	0.40	0.31	0.43	0.41	0.32
502–945 m	0.28	0.43	0.35	0.39	0.45	0.32
>945 m	0.41	0.40	0.36	0.49	0.48	0.32

BGD
4, 1279–1327, 2007

EGU

Table 2. Annual mean dissolved iron concentrations (nM) from selected ocean basins and depths from the simulations. For the simulations with no Fe release from dust (FeSed) or from the sediments (FeDust), and two simulations with no Fe release from desorption (NoDesorp), and with elevated desorption release (HighDesorp). Also shown is results from LowFe simulations with lower Fe inputs and scavenging losses (see text for details). Values in parentheses show the % difference from the New BEC simulation.

	Old	New	SedOnly	DustOnly	NoDesorp	LowFe	HighDesorp
N. Indian							
0–103 m	0.77	0.98	0.40 (–60)	0.81 (–18)	0.96 (–1.5)	0.66 (–33)	0.98 (+0.082)
103–502 m	0.63	0.77	0.37 (–52)	0.67 (–13)	0.73 (–4.8)	0.61 (–22)	0.78 (+0.97)
502–945 m	0.64	0.78	0.41 (–48)	0.73 (–7.1)	0.74 (–5.1)	0.60 (–23)	0.79 (+1.3)
>945 m	0.63	0.91	0.48 (–47)	0.86 (–6.1)	0.85 (–7.3)	0.65 (–29)	0.92 (+0.77)
N. Atlantic							
0–103 m	0.68	0.79	0.22 (–72)	0.65 (–18)	0.78 (–1.6)	0.62 (–22)	0.79 (+0.11)
103–502 m	0.62	0.74	0.28 (–62)	0.64 (–13)	0.71 (–2.8)	0.61 (–18)	0.74 (+0.58)
502–945 m	0.63	0.70	0.31 (–57)	0.64 (–9.2)	0.68 (–4.1)	0.60 (–15)	0.71 (+1.0)
>945 m	0.61	0.79	0.43 (–45)	0.73 (–7.2)	0.73 (–7.7)	0.63 (–21)	0.80 (+0.90)
N. Pacific(>15° N)							
0–103 m	0.25	0.34	0.23 (–32)	0.091 (–73)	0.33 (–3.5)	0.21 (–39)	0.34 (+0.36)
103–502 m	0.39	0.50	0.27 (–26)	0.23 (–55)	0.47 (–6.0)	0.49 (–1.0)	0.50 (+4.2)
502–945 m	0.47	0.55	0.42 (–24)	0.30 (–45)	0.48 (–12)	0.59 (+8.3)	0.56 (+2.0)
>945 m	0.49	0.52	0.43 (–17)	0.34 (–33)	0.37 (–29)	0.54 (+4.0)	0.54 (+5.0)
Equatorial Pacific							
0–103 m	0.11	0.16	0.14 (–17)	0.030 (–82)	0.16 (–3.0)	0.14 (–14)	0.16 (–0.18)
103–502 m	0.26	0.24	0.18 (–26)	0.11 (–54)	0.22 (–9.3)	0.49 (+106)	0.24 (+0.92)
502–945 m	0.31	0.28	0.19 (–31)	0.22 (–55)	0.22 (–19)	0.59 (+115)	0.29 (+3.6)
>945 m	0.35	0.35	0.29 (–17)	0.22 (–38)	0.27 (–24)	0.52 (+48)	0.37 (+4.9)
Southern Ocean							
0–103 m	0.29	0.21	0.16 (–24)	0.12 (–43)	0.19 (–7.4)	0.35 (+70)	0.21 (+0.54)
103–502 m	0.39	0.33	0.27 (–20)	0.18 (–46)	0.28 (–15)	0.57 (+71)	0.34 (+2.5)
502–945 m	0.43	0.36	0.28 (–23)	0.19 (–47)	0.27 (–26)	0.60 (+67)	0.38 (+5.5)
>945 m	0.45	0.46	0.39 (–15)	0.32 (–32)	0.33 (–29)	0.59 (+29)	0.59 (+5.7)

BGD
4, 1279–1327, 2007

EGU

Table 3. Global scale fluxes from the New BEC simulation are compared with the simulations with Fe inputs only from the sediments (SedOnly), with iron inputs only from dust (DustOnly), and with the LowFe and HighDesorp simulations (see text for details). The percentage change in flux relative to the New simulation is shown in parentheses. Fluxes listed include primary production (PP in PgC/yr), export production (ExpP sinking POC flux at 103 m in PgC/yr), nitrogen fixation (Nfix in TgN/yr), and water column denitrification (Denitr in TgN/yr). Also shown is the percentage of ocean area where iron is the limiting nutrient for each phytoplankton group (Diat%Fe – diatoms, Diaz%Fe – diazotrophs, and Sp%Fe – small phytoplankton).

	NewBEC	SedOnly	DustOnly	NoDesorp	LowFe	HighDesorp
PP	46.7	41.1 (–12)	44.5 (–4.6)	46.4 (–0.45)	45.37 (–2.7)	46.7 (0)
ExpP	5.75	4.90 (–15)	5.16 (–10)	5.71 (–0.82)	6.05 (+5.1)	5.75 (0)
Nfix	144	89.2 (–38)	94.6 (–34)	143 (–1.1)	127 (–12)	144 (0)
Diat%	34	58	59	36	14	34
Diaz%	36	59	65	37	46	36
Sp%	36	58	51	37	19	37

BGD
4, 1279–1327, 2007

Table 4. Residence time for dissolved iron from the New BEC simulation estimated as iron inventory/(loss due to sinking particulate flux + the 10% of scavenged iron that is presumed lost to the sediments). For the whole ocean domain this scavenging is the only loss term. We subdivide the ocean into areas with high and low iron inputs based on the annual mean surface concentration for iron, where high iron regions have surface concentration >0.55 nM and low iron regions are <=0.55 nM.

Depth-Area Considered	Residence Time (Years)
Upper 103 m Global	0.73
Upper 103 m High Iron	0.59
Upper 103 m Low Iron	1.3
Upper 502 m Global	2.0
Upper 502 m High Iron	1.3
Upper 502 m Low Iron	4.2
All Depths Global	15
All Depths High Iron	7.0
All Depths Low Iron	35

BGD
4, 1279–1327, 2007

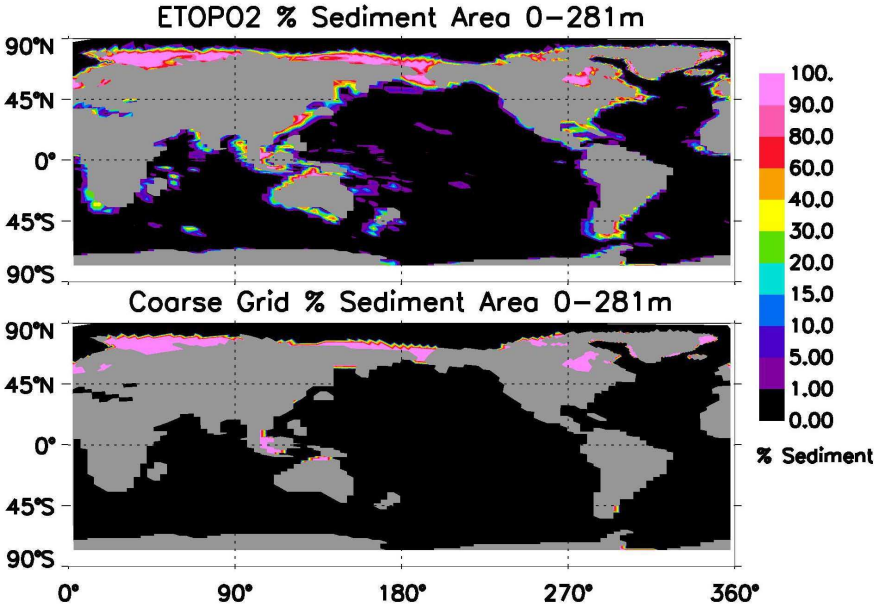

Fig. 1. Figure displays the percentage of grid cell area that would consist of ocean sediments (integrated over the upper 281m) in the ETOP2V2 database that is used in estimating the sedimentary source of dissolved iron **(a)**. Also, shown is the areas with depths less than 281m on the coarse resolution ocean grid **(b)**.

BGD
4, 1279–1327, 2007

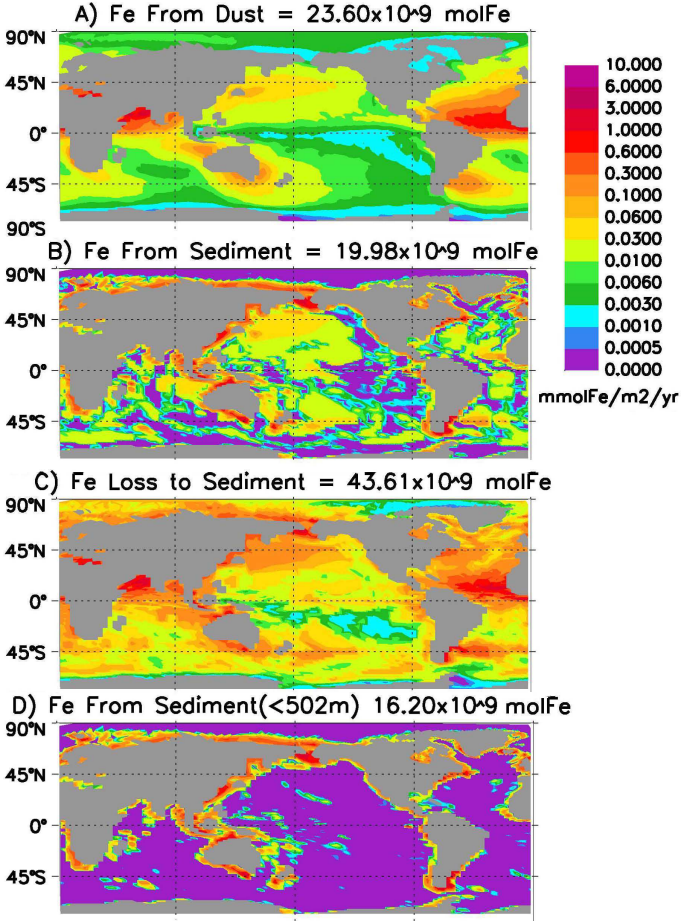

Fig. 2. Water column integrated input of dissolved iron from mineral dust **(A)** and from the sediments **(B)**, the loss of scavenged iron to the sediments **(C)**, and the sedimentary source of dissolved iron in the upper 502 m **(D)**.

BGD
4, 1279–1327, 2007

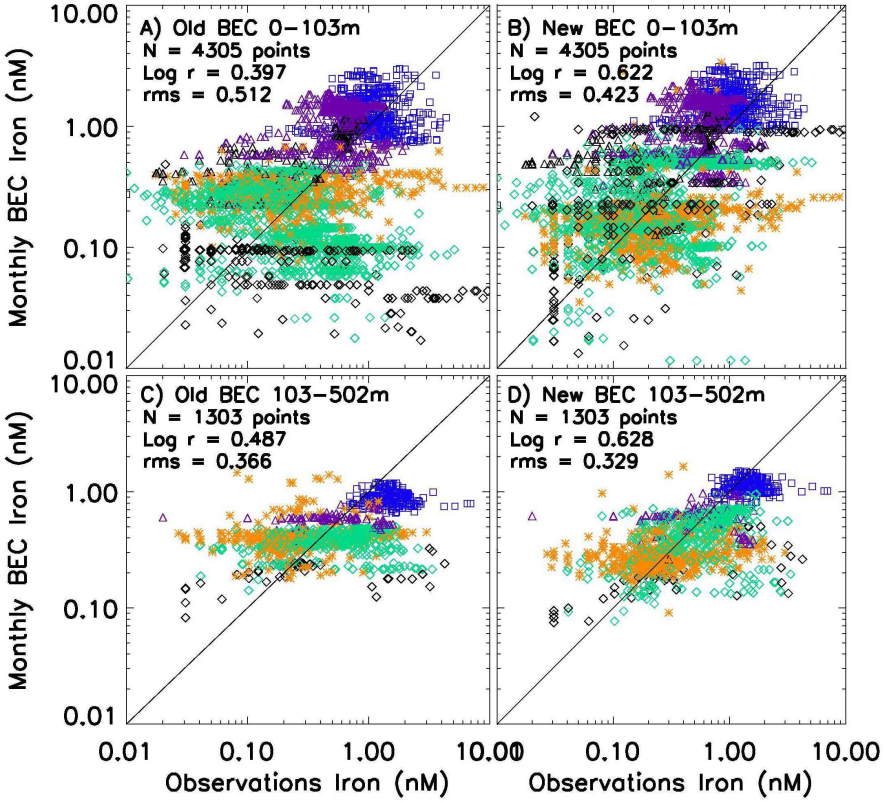

Fig. 3. Comparison of ocean measurements of dissolved iron with model output sub-sampled at the same month, location, and depth of the field observations for the Old BEC and New BEC simulations in surface waters (0–103 m, panels **A** and **B**) and in subsurface waters (103–502 m, panels **C** and **D**). Symbol shape and color indicate the ocean basin of the observation (N. Pacific – green diamonds, S. Pacific – black diamonds, N. Atlantic – purple triangles, S. Atlantic – black triangles, N. Indian – blue squares, S. Indian – black squares, and Southern Ocean (>40.5° S) – orange asterisks).

BGD
4, 1279–1327, 2007

EGU

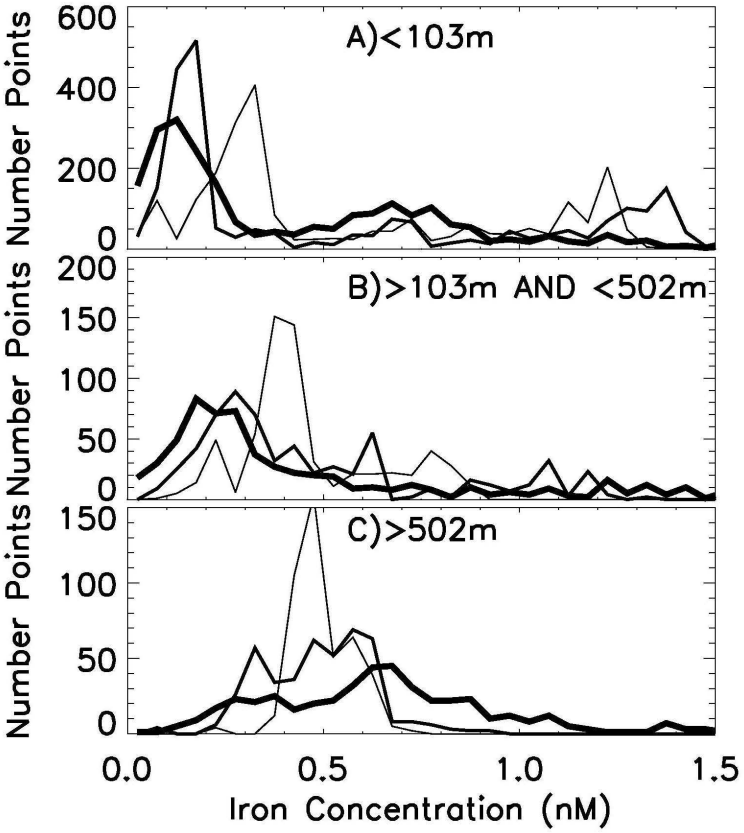

Fig. 4. Binned iron concentration values from the observations (thickest line), the New BEC simulation (medium line), and from the Old BEC simulation (thin line) over depth ranges of 0–103 m **(A)**, 103–502 m **(B)**, and from greater than 502 m **(C)**.

BGD
4, 1279–1327, 2007

EGU

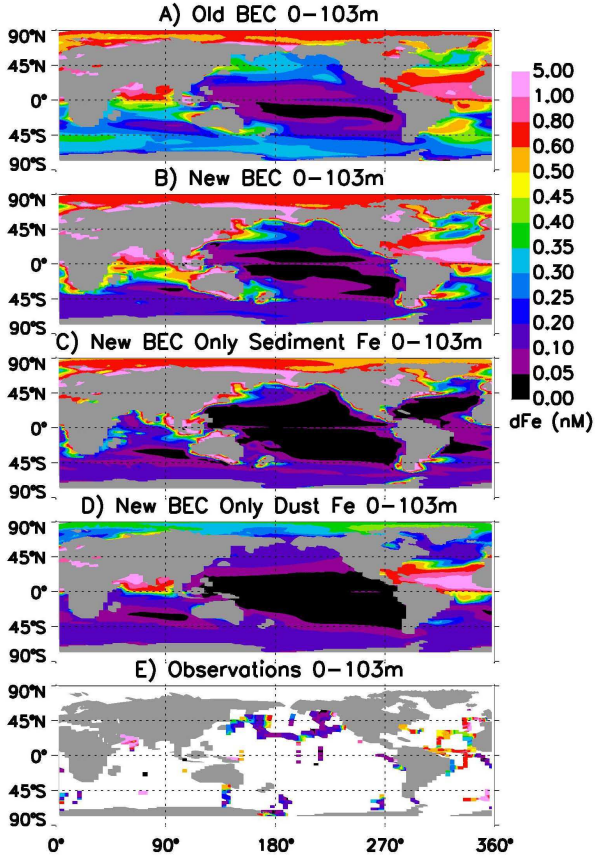

Fig. 5. Annual mean iron concentrations in the upper ocean (0–103 m) are shown for the Old BEC **(A)**, New BEC **(B)**, SedOnly **(C)**, and DustOnly **(D)** simulations with the iron observations averaged onto the model grid over this depth range **(E)**.

BGD
4, 1279–1327, 2007

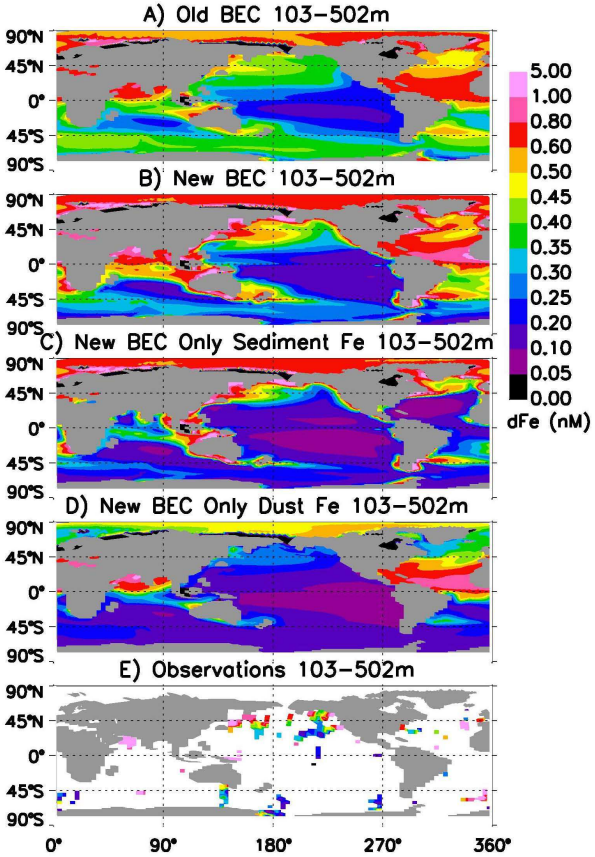

Fig. 6. Annual mean iron concentrations in the subsurface ocean (103–502 m) are shown for the Old BEC **(A)**, New BEC **(B)**, SedOnly **(C)**, and DustOnly **(D)** simulations with the iron observations averaged onto the model grid over this depth range **(E)**.

BGD
4, 1279–1327, 2007

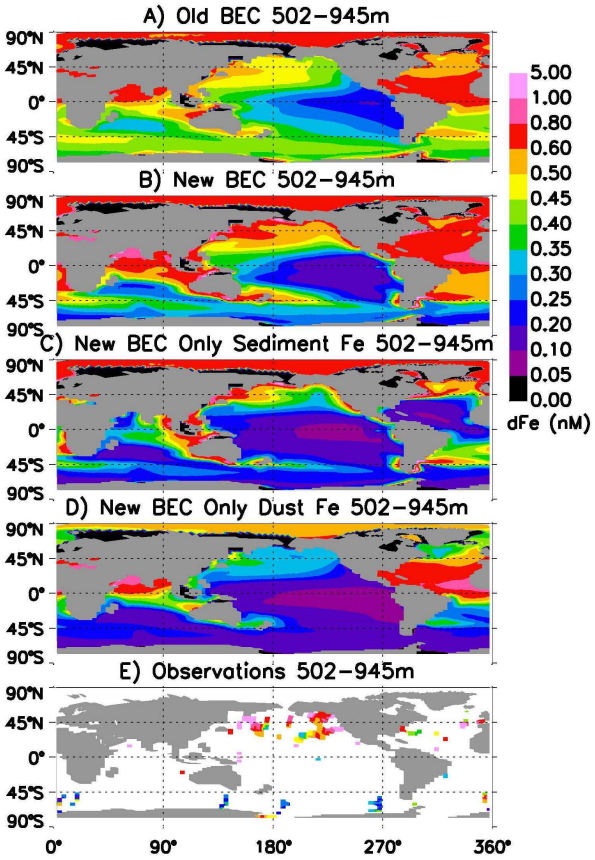

Fig. 7. Annual mean iron concentrations in the mid-depth ocean (502–945 m) are shown for the Old BEC **(A)**, New BEC **(B)**, SedOnly **(C)**, and DustOnly **(D)** simulations with the iron observations averaged onto the model grid over this depth range **(E)**.

BGD
4, 1279–1327, 2007

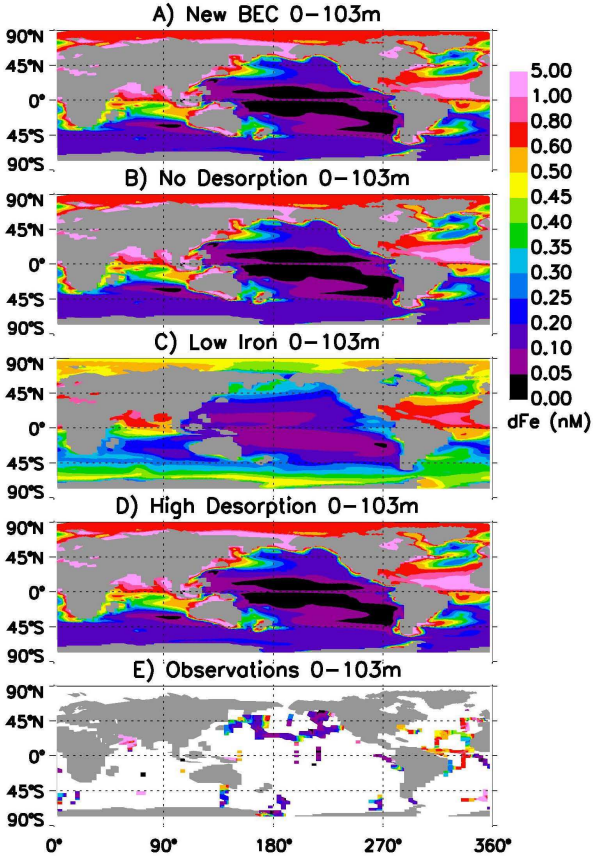

Fig. 8. Annual mean iron concentrations in the upper ocean (0–103 m) are shown for the New BEC **(A)**, NoDesorp **(B)**, LowFe **(C)**, and HighDesorp **(D)** simulations with the iron observations averaged onto the model grid over this depth range **(E)**.

BGD
4, 1279–1327, 2007

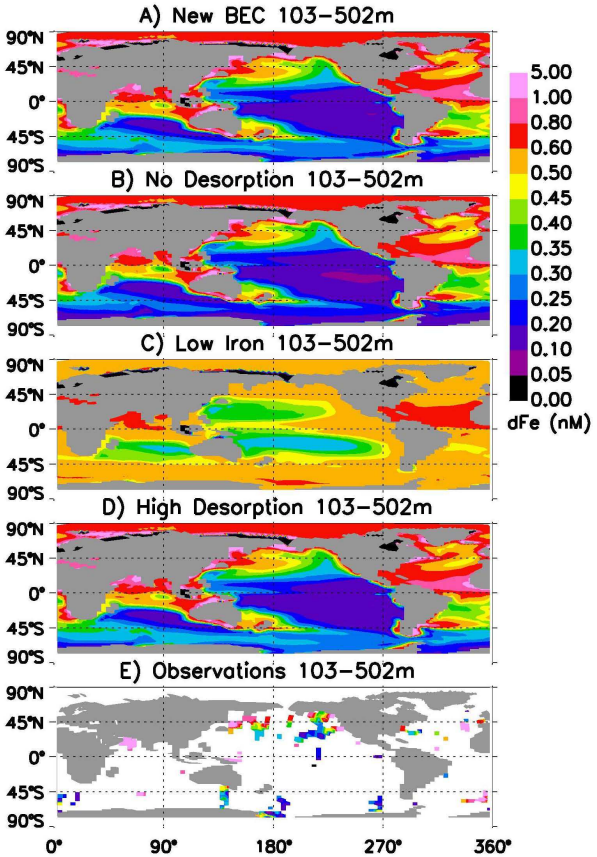

Fig. 9. Annual mean iron concentrations in the subsurface ocean (103–502 m) are shown for the New BEC **(A)**, NoDesorp **(B)**, LowFe **(C)**, and HighDesorp **(D)** simulations with the observations averaged onto the model grid over this depth range **(E)**.

BGD
4, 1279–1327, 2007

EGU

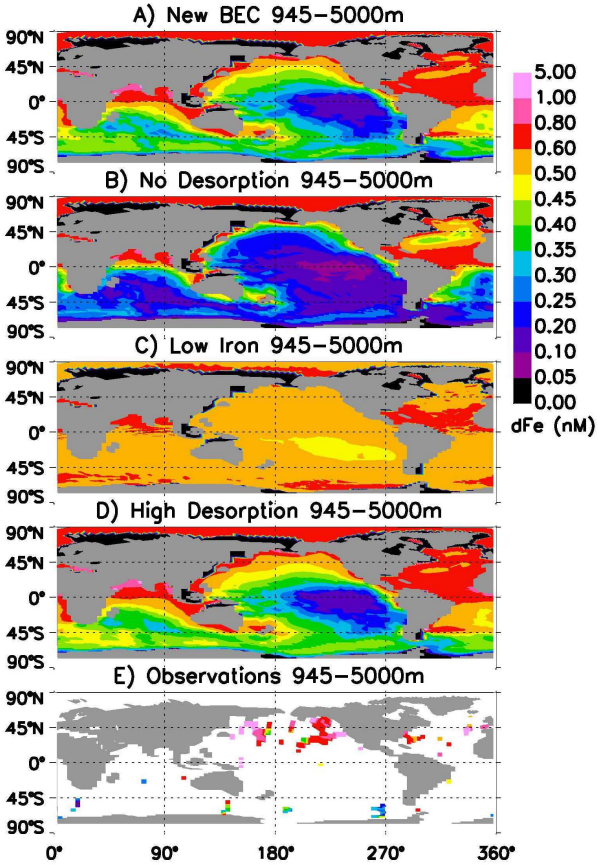

Fig. 10. Annual mean iron concentrations in the deep ocean (>945 m) are shown for the New BEC **(A)**, NoDesorp **(B)**, LowFe **(C)**, and HighDesorp **(D)** simulations with the iron observations averaged onto the model grid over this depth range **(E)**.

BGD
4, 1279–1327, 2007